

ORIGINAL ARTICLE

MIR137 schizophrenia-associated locus controls synaptic function by regulating synaptogenesis, synapse maturation and synaptic transmission

Enqi He¹, Miguel A. Gonzalez Lozano³, Sven Stringer⁴, Kyoko Watanabe⁴, Kensuke Sakamoto^{5,6}, Frank den Oudsten², Frank Koopmans¹, Stephanie N. Giamberardino^{5,6}, Anke Hammerschlag⁴, L. Niels Cornelisse², Ka Wan Li³, Jan van Weering², Danielle Posthuma⁴, August B. Smit³, Patrick F. Sullivan^{5,6,†} and Matthijs Verhage^{1,2,*,†}

¹Department of Functional Genomics, ²Department of Clinical Genetics, ³Department of Molecular and Cellular Neurobiology, ⁴Department of Complex Trait Genetics, Center for Neurogenomics and Cognitive Research (CNCR), Amsterdam Neuroscience, VU University Amsterdam and VU Medical Center, 1081 HV Amsterdam, The Netherlands, ⁵Department of Medical Epidemiology and Biostatistics, Karolinska Institutet, Nobels väg 12A, 171 77 Stockholm, Sweden and ⁶Department of Genetics, Center for Psychiatric Genomics, University of North Carolina at Chapel Hill, NC, USA

*To whom correspondence should be addressed. Tel: +31 (0) 20 59 86925; Fax: +31 20 598 92 81; Email: matthijs@cncr.vu.nl

Abstract

The *MIR137* locus is a replicated genetic risk factor for schizophrenia. The risk-associated allele is reported to increase miR-137 expression and miR-137 overexpression alters synaptic transmission in mouse hippocampus. We investigated the cellular mechanisms underlying these observed effects in mouse hippocampal neurons in culture. First, we correlated the risk allele to expression of the genes in the *MIR137* locus in human postmortem brain. Some evidence for increased *MIR137HG* expression was observed, especially in hippocampus of the disease-associated genotype. Second, in mouse hippocampal neurons, we confirmed previously observed changes in synaptic transmission upon miR-137 overexpression. Evoked synaptic transmission and spontaneous release were 50% reduced. We identified defects in release probability as the underlying cause. In contrast to previous observations, no evidence was obtained for selective synaptic vesicle docking defects. Instead, ultrastructural morphometry revealed multiple effects of miR-137 overexpression on docking, active zone length and total vesicle number. Moreover, proteomic analyses of neuronal protein showed that expression of *Syt1* and *Cplx1*, previously reported as downregulated upon miR-137 overexpression, was unaltered. Immunocytochemistry of synapses overexpressing miR-137 showed normal Synaptotagmin1 and Complexin1 protein levels. Instead, our proteomic analyses revealed altered expression of genes involved in synaptogenesis. Concomitantly, synaptogenesis assays revealed 31% reduction in synapse formation. Taken together, these data show that miR-137 regulates synaptic function by regulating synaptogenesis, synaptic

[†]Equivalent contributions.

Received: December 28, 2017. Revised: February 15, 2018. Accepted: February 17, 2018

© The Author(s) 2018. Published by Oxford University Press.

This is an Open Access article distributed under the terms of the Creative Commons Attribution Non-Commercial License (<http://creativecommons.org/licenses/by-nc/4.0/>), which permits non-commercial re-use, distribution, and reproduction in any medium, provided the original work is properly cited. For commercial re-use, please contact journals.permissions@oup.com

ultrastructure and synapse function. These effects are plausible contributors to the increased schizophrenia risk associated with miR-137 overexpression.

Introduction

Schizophrenia is a common psychiatric disorder of high heritability (1). Our knowledge of genetic factors contributing to schizophrenia risk is progressing, and there are now many replicated, genome-wide significant loci (2). One of the best replicated loci centers around the single nucleotide polymorphism (SNP) rs1625579 located in an intron of microRNA (miRNA) gene *MIR137* (2,3). This locus is also part of 1p21.3 deletions that give rise to intellectual disability (4). The shortest region of overlap among these microdeletions includes *MIR137*. miRNAs are small non-coding RNA molecules, which bind target mRNAs, modulate their activity and half-life and regulate protein expression at the post-transcriptional level (5). The schizophrenia-associated SNPs were reported to produce higher miR-137 levels (6). Changes in miRNA expression can influence the expression of hundreds of proteins directly or indirectly, and generate pleiotropic effects on structure and function of the cells in which their expression is altered. Given this broad action radius of miRNAs, genetic variation that alters expression of miRNA genes may contribute to vulnerability for disease.

miR-137 is expressed in embryonic and adult brain (7,8) and enriched in hippocampus (4,9,10). Knockout of *MIR137* results in early embryonic lethality in mouse (11). However, microarray analysis did not detect miR-137 expression in rat cultured hippocampal neurons (12). Target prediction has identified many genes potentially regulated by miR-137 expression (13–19). Several genes associated with schizophrenia are among the putative targets (2) and four (*CSMD1*, *C10orf26*, *CACNA1C* and *TCF4*) have been validated as miR-137 targets in HEK-293 cells (20). Hence, dysregulation of miR-137 expression is a plausible contributor to schizophrenia risk.

Down-regulation of miR-137 expression in a neuroendocrine cell line alters expression of genes involved in synaptogenesis and synaptic transmission (17). miR-137 inhibition [via expressing the multiple reverse complement sequence of mature miR-137 (Sponge miR-137).] (21) decreased the number of silent synapses and potentiated synaptic transmission by upregulating AMPA receptor expression and function (22). Moreover, down-regulation of miR-1000, which has a similar seed sequence to miR-137, in *Drosophila*, inhibited synaptic transmission by decreasing VGLUT2 expression (23). Hence, several studies suggest that decreased miR-137 expression, i.e. an effect opposite of what the disease-associated genetic variation is reported to do (6), promotes synapse formation and function.

Conversely, upregulation of miR-137 expression was reported to reduce proliferation and stimulate differentiation in embryonic neuronal stem cells and brain tumor cells (7,9). However, the opposite phenotype (promoting proliferation) was observed for adult neuronal stem cells (24). Furthermore, over-expression of miR-137 in primary cultured neurons inhibited neuron development by downregulating *Mind Bomb-1* (*Mib1*) (10). *In vivo* experiments in mice showed that miR-137 over-expression impaired long-term potentiation (LTP), learning and memory. This deficit was attributed to pre-synaptic dysfunction: altered docking of synaptic vesicles, reduced synaptic transmission and reduced expression of pre-synaptic proteins (6). The same study reported a 30% reduction of synaptotagmin-1 (*Syt1*) levels, with synaptic dysfunctions rescued by acute *Syt1*

over-expression (6). These studies suggested that higher expression of miR-137 generally produces opposite effects to those of lower expression, inhibiting neuronal development, LTP and synaptic functions, possibly by a rather selective effect on the expression a few synaptic genes (*Mib1* or *Syt1*). However, it remains unclear how such modest changes in the expression of pre-synaptic proteins produce such robust effects on synapse organization and function.

Therefore, we investigated the molecular mechanisms of miR-137-induced synaptic changes in primary cultured hippocampal neurons. Since upregulation of miR-137 is the most relevant effect associated with schizophrenia (6), we over-expressed miR-137 and characterized changes in synaptogenesis, synaptic ultrastructure, synaptic transmission and protein composition of the synapse. We confirmed that over-expression of miR-137 impaired synapse organization and function. However, our data indicate that this is due to a multitude of effects on many morphological, ultrastructural and functional parameters, such as total number of synapses formed, dendritic length, total number of vesicles per synapse, active zone length, altered expression of >30 synaptic proteins (but not *Syt1*), reduced release probability and short-term plasticity. Alterations in synaptic transmission were not rescued by *Syt1* over-expression. Hence, miR-137 regulates synaptic function by pleiotropic effects on synaptogenesis, synaptic ultrastructure and synapse function. These effects are plausible contributors to the increased schizophrenia risk associated with miR-137 overexpression.

Results

Fine mapping of associated *MIR137* locus reveals 3 candidate genes

First, we inspected the Psychiatric Genomics Consortium (PGC) schizophrenia genome-wide association study (GWAS) results (2) in the associated locus using Locuszoom (Fig. 1A and B) (Pruim et al., 2010). This locus (chr1: 98.30–98.55Mb) contains the schizophrenia-associated SNPs rs1198588, rs1625579, rs2660304 and rs2802535 (6). On the 5' side, the boundary of the associated region is rather sharp, with a clear loss of association between 98.55–98.60Mb, well before the location of the adjacent gene (*LOC7729987*). On the 3' side, the border of the associated region is less well defined and association runs into the adjacent *DPYD* gene (Fig. 1A). The associated locus contains the *MIR137* host gene (*MIR137HG*), a RNA gene containing the miR-137 miRNA and a second miRNA (*MIR2682*) with no known function (Fig. 1B). Second, we aligned the GWAS results with the expression results from genotype-tissue expression (GTEx) and analyzed correlations between the schizophrenia risk variant and gene expression across eight brain regions (Lonsdale et al., 2013). We observed some evidence for increased expression of the host gene, *MIR137HG*, in hippocampus of carriers of the disease-associated genotype, and to a lesser extent also in caudate putamen/basal ganglia (Fig. 1C), but not in other brain regions relevant for schizophrenia, such as the cortex, hypothalamus and the rest of the basal ganglia, nor in testis, pituitary, ovary, cell transformed fibroblasts and adrenal. Because the risk-associated allele was also previously shown to increase

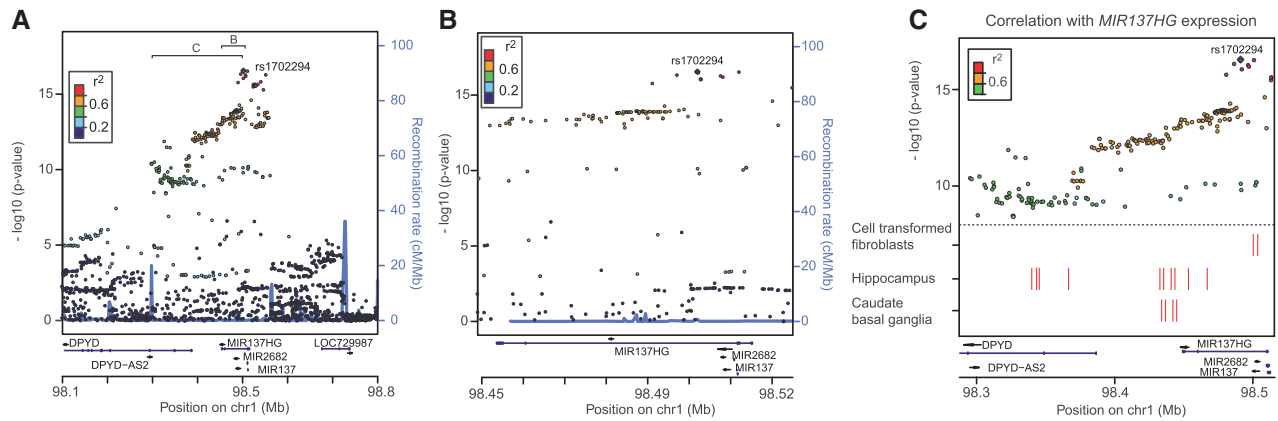


Figure 1. Genetic evidence of *MIR137* region in humans associated with schizophrenia (A) Schizophrenia GWAS hits and genes located on chromosome 1 between 98.1 and 98.8 Mb (genome build hg19). The genomic region shown in (B) and (C) are indicated with B and C at the top of (A). (B) Schizophrenia GWAS hits and genes located in *MIR137* region. (C) Association between 206 schizophrenia risk variants near *MIR137* (i.e. those with $r^2 > 0.6$ within the region of GWAS top SNP rs1702294) and expression of *MIR137HG* in 10 tissues, cells and brain regions (testis, ovary, adrenal, cell transformed fibroblasts, basal ganglia, hypothalamus, hippocampus, cortex and caudate putamen basal ganglia). Three tissues show some evidence for association between the schizophrenia risk variant and higher expression of *MIR137HG* ($t > 2.5$; $P_{\min} = 0.0056$). The associated SNPs are re-plotted from (A) for clarity.

miR-137 expression (6), we went on to characterize the mechanisms underlying the synaptic defects induced by miR-137 over-expression in mouse hippocampal neurons.

miR-137 over-expression reduces basal synaptic transmission and alters short-term plasticity

Previous experiments in hippocampal slices found that miR-137 over-expression inhibits synaptic transmission and plasticity (6). We tested this in a standardized assay using single hippocampal neurons grown on micro-dot astrocyte islands (25,26) and verified miR-137 levels after lenti viral over-expression by qPCR. Whole-cell patch clamp recordings of synaptic transmission revealed a 50% reduction in evoked excitatory post-synaptic current (EPSC) amplitude in miR-137 over-expressing neurons compared with control neurons expressing a scrambled sequence (Fig. 2A and B). The spontaneous release (mEPSC) frequency was reduced to 50% of the scramble control, but not the mEPSC amplitude (Fig. 2C–E). Paired pulse stimulation showed strong facilitation in miR-137 over-expressing neurons but not in control neurons (Fig. 2F). miR-137 over-expressing neurons also showed earlier rundown than the scramble group during repetitive stimulation (Fig. 2G), but similar asynchronous release (Fig. 2H). Taken together, the low evoked EPSC, the decreased mEPSC frequency and the facilitation during paired pulse tests suggest a reduction in the number of active synapses and additional defects in active synapses, especially a decreased release probability, in miR-137 over-expressing neurons. The different paired pulse response and the unaltered mEPSC amplitude suggest a selective pre-synaptic deficit.

Since exogenously expressed Syt1 rescued deficits in synaptic transmission caused by miR-137 upregulation *in vivo* (6), we performed similar rescue experiments. After over-expression, Syt1 level was significantly increased (Fig. 2N and O). However, in our test conditions, Syt1 over-expression did not rescue synaptic transmission deficits caused by miR-137 over-expression (Fig. 2I–M). Hence, our data indicate that miR-137 regulates synaptic transmission by altering pre-synaptic release and possibly synapse formation, but loss of Syt1 function is not the sole cause of these deficits.

miR-137 over-expression changes many aspects of synaptic ultrastructure

Impaired pre-synaptic release could arise from ultrastructural changes in the active zone (6). We used electron microscopy to analyze the ultrastructure of synapses (Fig. 3A). As reported previously, miR-137 over-expressing neurons showed a 30% reduction in active zone length and membrane-proximal (docked) vesicles (6). We also found a 29% reduction in active zone length (Fig. 3B) and 28% reduction in post-synaptic density (PSD) (Fig. 3E). Meanwhile, the synaptic vesicle cluster size reduced 37% (Fig. 3F), total number of synaptic vesicles reduced 39% (Fig. 3G) and the number of docked synaptic vesicles reduced 34% (Fig. 3C). Consequently, the number of docked vesicles per active zone length was unchanged, but the distribution of synaptic vesicle at synapses is (Fig. 3D). A 43% reduction of large dense core vesicles (LDCVs) per synapse was observed (Fig. 3H). Hence, we confirm the previously observed reduction in membrane-proximal (docked) vesicles upon miR-137 over-expression, but that this change is part of pleiotropic changes in pre-synaptic structure upon miR-137 over-expression, which likely contributes to the observed changes synaptic transmission.

miR-137 over-expression alters expression of proteins involved in synaptogenesis

To investigate changes in protein levels that may help to explain functional and ultrastructural effects of miR-137 over-expression, we performed proteomics analysis of a total protein sample from primary cultured DIV17 hippocampal neurons overexpressing miR-137 and scramble controls ($n = 6$). Proteins were resolved on a SDS polyacrylamide gel, digested with trypsin and peptides were identified and quantified by LC-MS/MS data-independent acquisition using SWATH (27). A total of 10 831 peptides were finally used for the identification and quantification of 2314 proteins, with a median coefficient of variation of 9 and 10% for the miR-137 overexpression and scramble control group, respectively. Comparison between groups revealed 43 proteins significantly regulated in abundance [empirical Bayes moderated t -statistics false discovery rate (FDR) ≤ 0.05]. Some known miR137 targets were found significantly

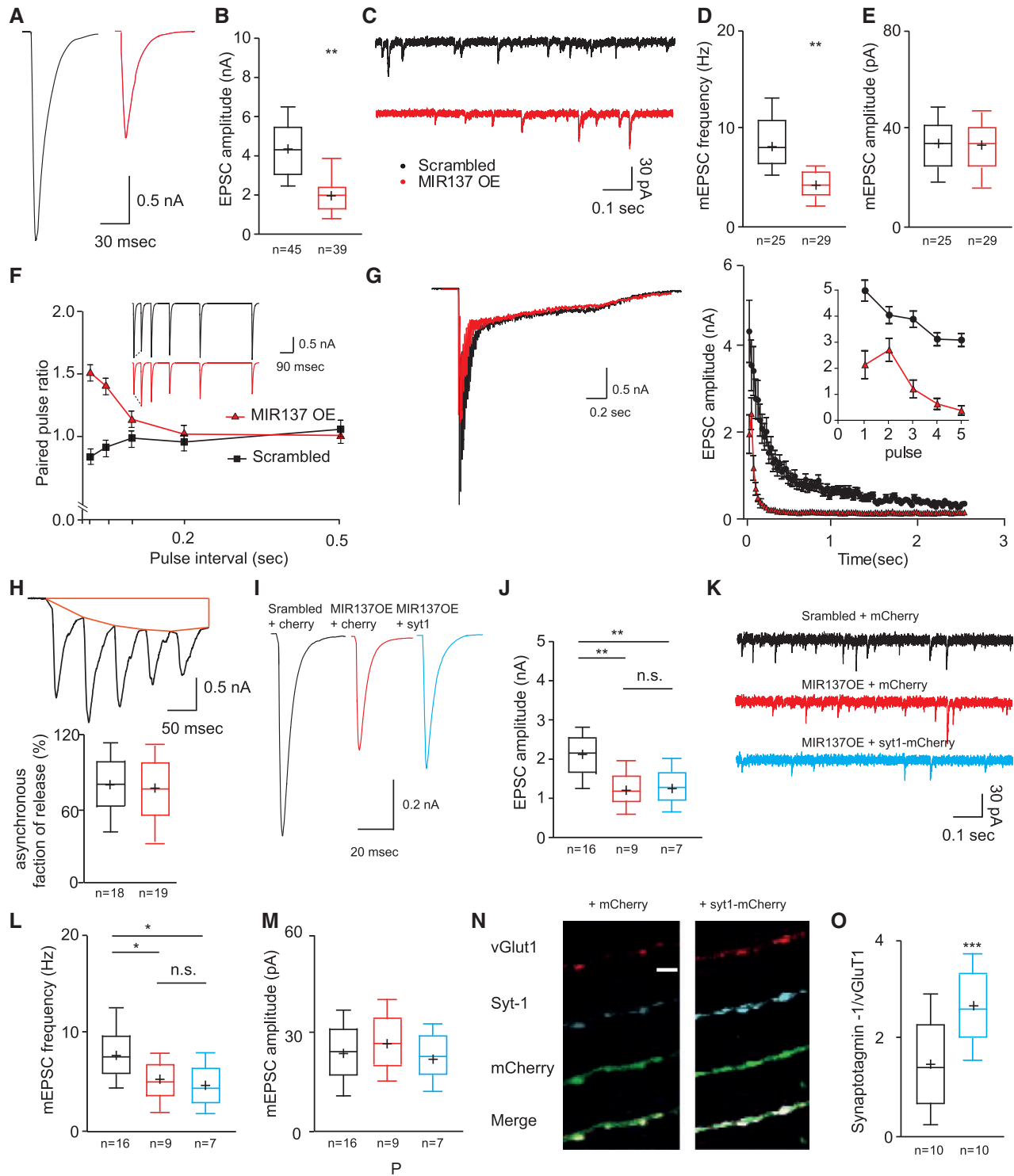


Figure 2. MIR137 over-expression changes synaptic transmission. Sample traces (A) and quantification of evoked EPSCs (B) in scrambled or MIR137 over-expressed neurons ($P = 0.003$, unpaired t-test). sample traces of miniature EPSC (C), and quantification of frequency ($P = 0.005$, unpaired t-test) (D) and amplitudes (E) in scrambled or MIR137 over-expressing neurons. (F) Sample trace and quantification of paired pulse ratio (PPR). (G) Sample trace and quantification of EPSC size depression during repetitive stimulation at 40 Hz. (H) Asynchronous fraction of release is obtained from normalizing asynchronous charge to total release charge. The sample trace (red area) represents the asynchronous charge from the first five pulses in train stimuli. sample traces (I) and quantification of evoked EPSCs (J) in scrambled or MIR137 OE group with Syt1 over-expressed neurons ($P = 0.008$, ANOVA). sample traces of miniature EPSC (K), and quantification of frequency ($P = 0.031$, 0.030, ANOVA) (L) and amplitudes (M) in scrambled or MIR137 OE group with Syt1 over-expressing neurons. (N) Typical sample images of WT neurons over-expressing synaptotagmin-1-mCherry or mCherry (control). The scale bar is 40 μm. (O) The over-expression level of Syt1 at the synapse, compared between control and over-expression group ($P = 0.0004$, unpaired t-test). In all boxplots, the lower and upper quartile represent observation outside of the 25–75 percentile range. The lower and upper whiskers represent the 10–90 percentile range. The boxes also show the median (–) and mean (+). * $P < 0.05$, ** $P < 0.01$, *** $P < 0.001$.

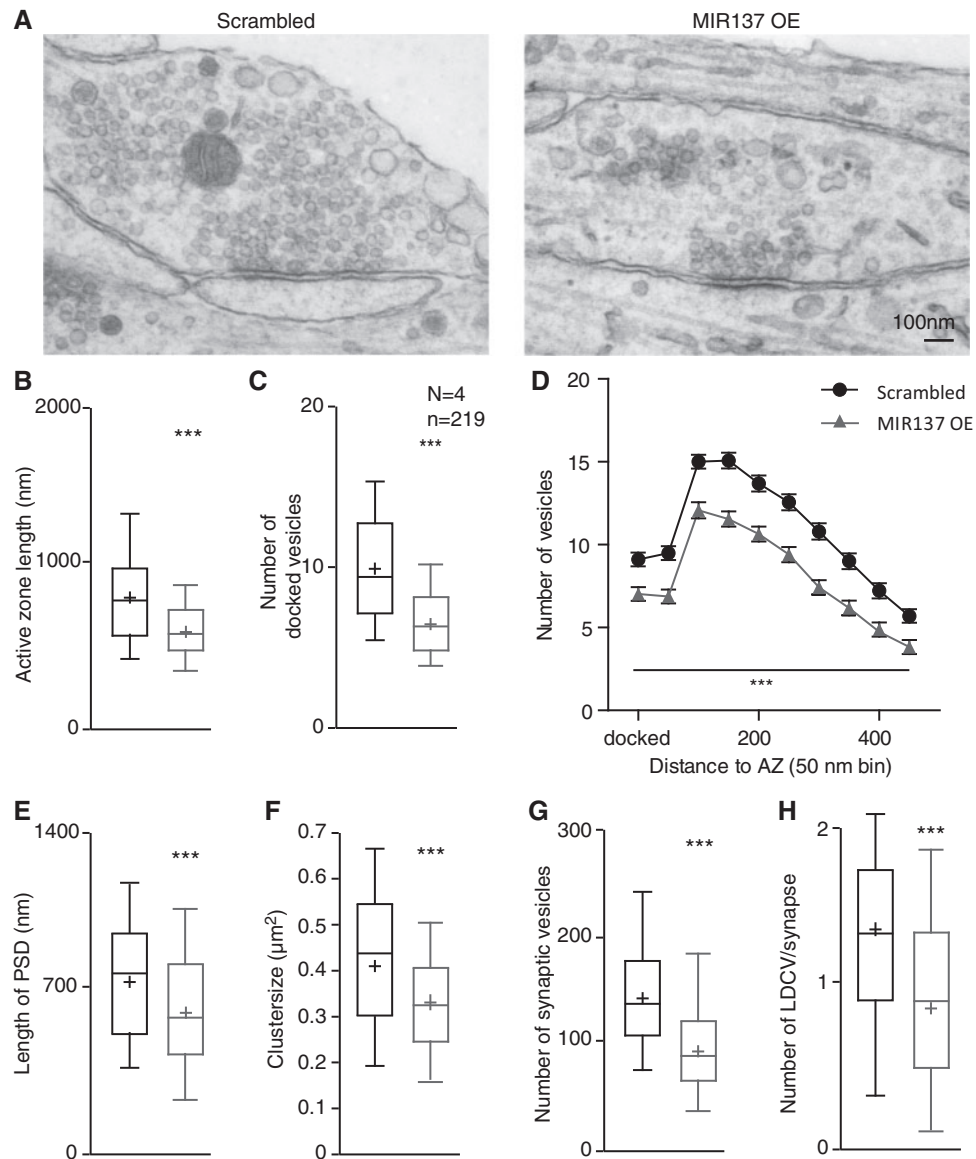


Figure 3. *MIR137* overexpression alters pre-synaptic ultrastructure (A) Electron micrographs of typical asymmetrical glutamatergic synapses from neurons over-expressing scrambled constructs or *MIR137*. Comparing active zone size, $P = 1.25e^{-13}$ (B), number of docked vesicles, $P = 3.84e^{-17}$ (C), distribution of synaptic vesicles (D), post-synaptic density (PSD) size, $P = 3.11e^{-15}$ (E), vesicle cluster size, $P = 1.64e^{-14}$ (F), total number of synaptic vesicles, $P = 2.09e^{-16}$ (G), number of LDCVs per synapse, $P = 1.37e^{-5}$ (H) between scramble and *MIR137* over-expression neurons. In all boxplots, the lower and upper quartile represent observation outside of the 25–75 percentile range. The lower and upper whiskers represent the 10–90 percentile range. The boxes also show the median (–) and mean (+). * $P < 0.05$, ** $P < 0.01$, *** $P < 0.001$ as determined by multilevel test.

regulated, e.g. NFASC, EDIL3, SYNCRIP, DDX3X showing a reduction in expression level when overexpressing *MIR137*, as expected (28). The proteins significantly changed by overexpression of *miR-137* were enriched for cell adhesion and cell development proteins (Fig. 4A). For *Syt1*, complexin-1 and neuroligin-3, the results from the mass spectrometry experiments were confirmed by Western blotting (Fig. 4B). Thus, *miR-137* overexpression altered a limited number of proteins, especially proteins involved in synapse development, but not the previously reported proteins *Syt1*, complexin1 and NSF (6). To identify *MIR137* targets, we compared the number of proteins significantly up/downregulated in our proteomics experiments to *MIR137* putative target genes from mRNA analyses in previous studies. Little overlap was observed among all studies published so far and the current study (Fig. 4C and D).

miR-137 over-expression suppresses synapse formation in cultured neurons

To test the suggestion that *miR-137* regulates neuronal development and synapse formation, we analyzed neuronal proliferation and synapse formation *in vitro*. The number of synapses formed per neuron was obtained by semi-automatic counting on synapses indicated by vesicular glutamate transporter-1 (vGlut1) staining, and dendritic morphology was assessed using microtubule-associated protein 2 (MAP2) staining at DIV 17 (Fig. 5A). Over-expression of *miR-137* at early developmental stages (DIV 0) significantly reduced synapse number, dendrite length and synapse density (Fig. 5B–D). Sholl analysis demonstrated an abnormal distribution of synapses along the dendrite compared with the scramble control group (Fig. 5H). We also stained for several synaptic proteins such as complexin1/2,

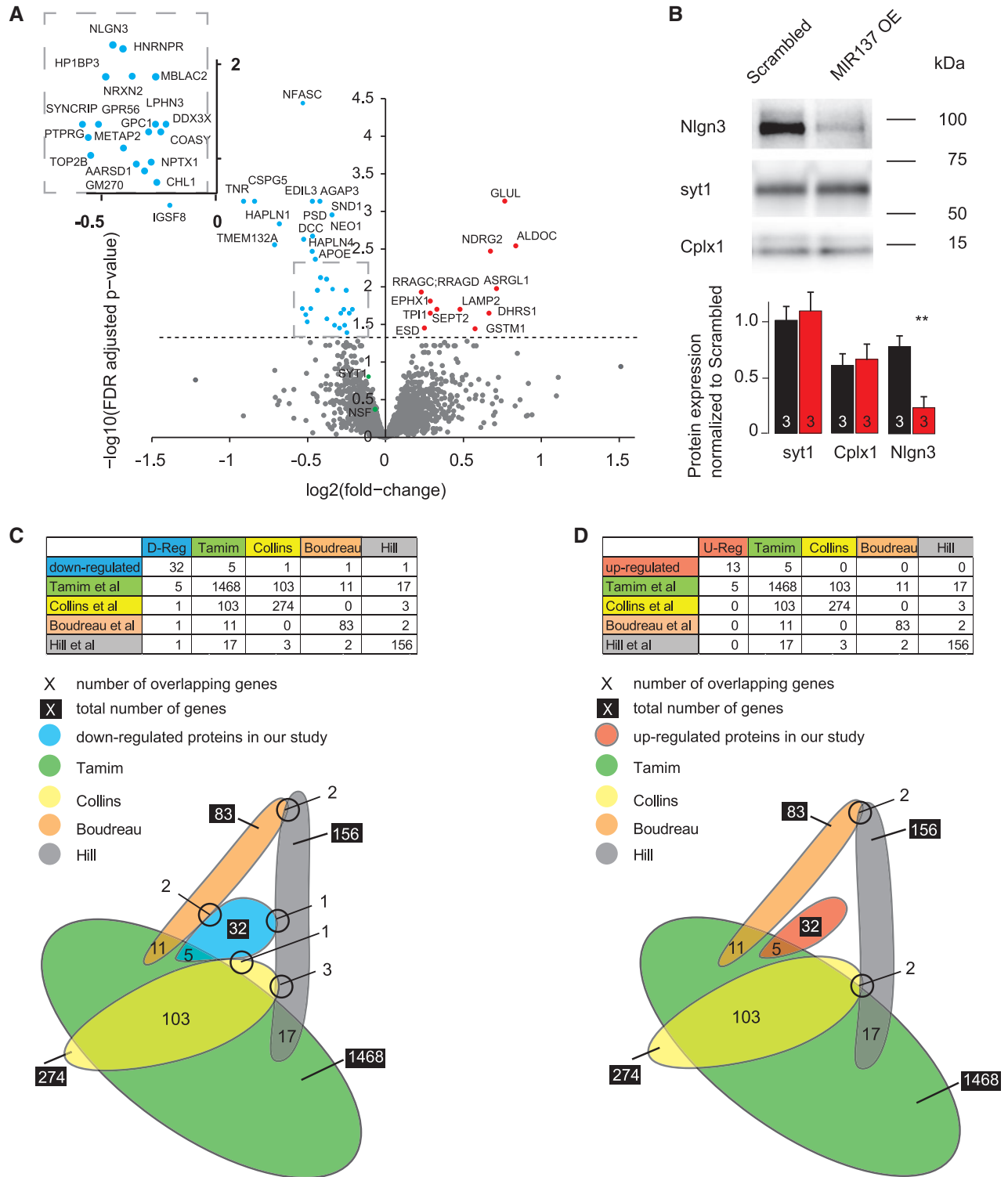


Figure 4. MIR137 over-expression alters expression of synaptic genes with little overlap with previous studies. Proteomics analysis showed MIR137 over-expression affected a specific group of proteins. (A) Volcano plot shows the distribution of protein expression in primary cultured mice hippocampal neurons with MIR137 over-expression. Dots above the dash line represent expressed proteins show >20% change and a significant FDR adjusted P-value ($P \leq 0.05$). (B) Quantification of selected proteins levels in primary cultured mice hippocampal neurons for scrambled or MIR137 OE. ** $P < 0.01$, are determined by independent t-test. Comparison of previously proposed MIR137 targets (mRNA analyses in previous studies) to proteins found significantly downregulated (C) or upregulated (D) in our proteomics experiments. Downregulated proteins in the current study are indicated in blue (C) and the upregulated in red (D). Previous studies: green [(18) RNA data]; yellow [(14) RNA data]; gray [(15) RNA]; brown [(13) RNA]. The total number of genes/proteins in each group is indicated in a black box. The number of genes/proteins overlapping between groups is indicated both in the diagrams and in the tables.

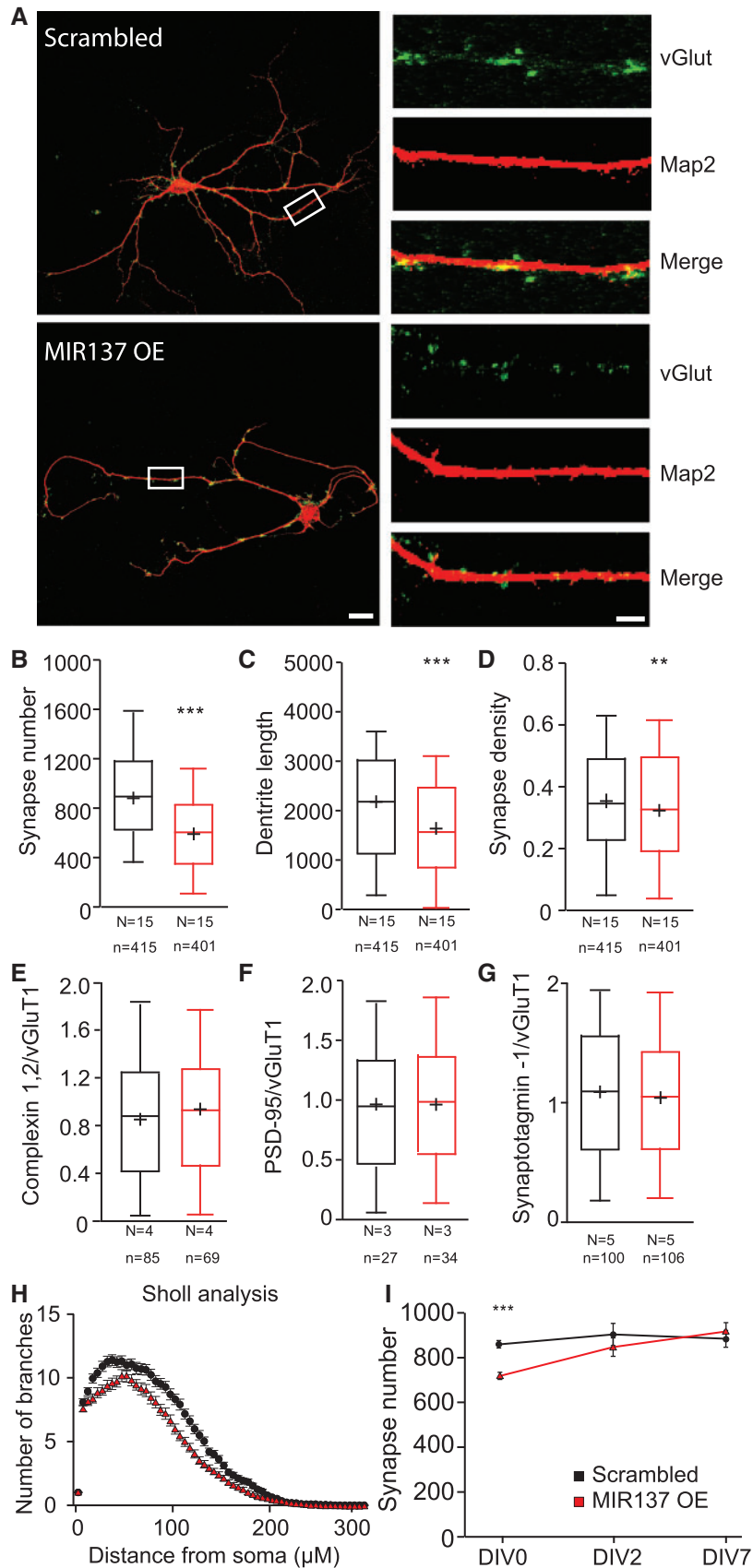


Figure 5. MIR137 over-expression reduces synaptogenesis and synapse maturation in a development dependent manner (A) Typical sample images of WT neurons infected with scramble or MIR137 viral particles at DIV 0 and stained for Map2 (dendritic marker) and vGluT1 (pre-synaptic terminal marker) at DIV 17. Length of the scale

PSD-95, synaptotagmin-1, munc18 and rab3 (Fig. 5E–G). The levels of these proteins were similar. At later stages (DIV2 and DIV7) over-expression miR-137 produced a more subtle effect (no significant) on synapse number and dendrite length (Fig. 5I). Consistent with the conclusions from experiments on autaptic neurons, over-expression miR-137 in primary cultured continental hippocampal neurons also showed a reduction of synapse density and dendrite length. Taken together, our results suggest that miR-137 regulates dendrite growth and synapse formation in a development dependent manner, which may explain most synaptic deficits.

Discussion

In this study, we modeled the possible pathological effects of increased miR-137 expression for schizophrenia by viral over-expression in cultured hippocampal neurons. The original evidence for altered miR-137 expression in relation to the genetic variation associated with schizophrenia was derived from *in vitro* experiments (6) and a recent study did not observe altered expression (29). On the other hand, GTEx data (30) contains several significant eQTLs (Fig. 1C). Furthermore, current methods to detect eQTLs (using postmortem material) have limited power to detect transient or local effects of genetic variation on gene expression, while such transient or local effects may be sufficient to explain the association with schizophrenia. Hence, while evidence in favor of altered expression in relation to schizophrenia awaits further study, (transient or locally) increased miR-137 expression appears to be a plausible scenario to explain the contribution of genetic variation in the MIR137 locus to schizophrenia risk. We observed that miR-137 over-expression produced a variety of pleiotropic effects: impaired synaptic transmission; decreased mini-frequency; altered short-term plasticity; impaired synaptic vesicle docking; decreased active zone size and total number of synaptic vesicles; altered expression of proteins involved in neuronal development and synapse formation; and reduced *in vitro* synapse formation and dendrite growth. Little overlap was found between published collections of genes observed or predicted to be regulated by miR-137 (13–19) and also between these collections and differentially expressed proteins in the current study. This lack of overlap may be explained by the fact that these studies used different model systems, e.g. stem cell, neuronal precursor, the human brain and glioblastoma cell lines, and different detection systems, e.g. RIP-seq and RNA-seq. Hence, for the correct interpretation of functional miR-137 effects, it is crucial to take into account the collection of regulated genes/proteins in the specific model system studied.

The current data confirm previous conclusions (6,23) that expression of miR-137 (or the seed-similar *Drosophila melanogaster* miRNA miR-1000) in mature neurons inhibits synapse function via pre-synaptic mechanisms. Several miRNAs are known to regulate synapse function specifically via post-synaptic mechanisms, such as miR-134, miR-181 and miR-223 (31–33). miR-137

now emerges as a mainly pre-synaptic regulator, together with miR-485 (34). Post-synaptic effects on glutamate receptor densities have been observed for miR-137 (22). However, in the current study no evidence for an altered receptor density in glutamatergic synapses was found (mEPSC amplitudes were normal, Fig. 2E). Despite some unresolved discrepancies, the picture emerges that miRNA expression is an effective biological principle to modulate synaptic function and that different miRNAs achieve this by targeting different sides of synapses. This suggests that miRNAs target mRNA collections enriched for either pre- or post-synaptic mRNAs and that such collections contain specific recognition sites for miRNAs to do so. The synaptic responses are toned by miRNAs, usually not just on/off but adapted established systems to new scenarios. However, with the current approaches (proteomics and bioinformatics) this prediction is not confirmed yet and divergent mRNA/protein collections are found/predicted to be regulated by miRNAs like miR-137 (see above and Fig. 4C and D).

Previous studies (6,23) reported specific mechanisms by which miR-137 regulates pre-synaptic function, via reduced Syt1 or vGlut2 expression, respectively. However, the current data, obtained in a reduced and highly standardized model system, suggest pleiotropic effects on synaptogenesis, pre-synaptic ultrastructure and function. Syt1 is the main calcium sensor for synaptic vesicle release in around half of all CNS neurons (35), and also involved in upstream steps in the regulated secretory pathway, such as local accumulation of secretory vesicles and their docking at the target membrane (36,37). Therefore, changes in Syt1 expression in principle provide a plausible explanation for the impaired pre-synaptic functions. Indeed, Syt1 over-expression rescued all deficits caused by miR-137 over-expression, including vesicle distribution, synaptic transmission, synaptic plasticity and learning behavior in mice (6). However, the reduction in Syt1 level was moderate (30%) in this study. It is difficult to explain how such a moderate reduction leads to such robust functional differences. For instance, no functional or behavioral abnormalities have been reported for Syt1 heterozygous mice, which have a 50% reduction in Syt1 expression. Furthermore, the effect on the number of vesicles upon miR-137 over-expression (30% reduced Syt expression) is larger than observed in Syt1 null mutant synapses (100% reduced Syt expression): a 17% reduction in the first 100nm upon miR-137 over-expression (6) versus a 15% reduction in the Syt1 null mutant (36). Finally, such relatively moderate effects on vesicle distribution are probably insufficient to explain the robust effects on synaptic transmission. For instance a mutant mouse with heterozygous null mutation for the pre-synaptic gene *munc18-1* showed a 33% reduction in vesicle docking while the evoked EPSC amplitude was unaffected (38). Hence, taken together, the moderate reduction in Syt1 expression does not appear to be sufficient as a sole explanation for the robust deficits in pre-synaptic function upon miR-137 over-expression. Moreover, we found no change in Syt1 or vGlut2 expression using three independent methods (mass spectrometry, Western blotting and

bar is 50 μ m. (B) Total synapse number is compared between scramble and MIR137 expressing neurons, $P = 0.0003$. (C) Dendritic length is compared between scramble and MIR137 expressing neurons $P = 0.0008$. (D) Synapse density is compared between scramble and MIR137 expressing neurons, $P = 0.007$. (E) Level of complexin 1, 2 at the synapse is compared between scramble and MIR137 expressing neurons. (F) Level of PSD-95 at the synapse is compared between scramble and MIR137 expressing neurons. (G) Level of Syt1 at the synapse is compared between scramble and MIR137 expressing neurons. (H) sholl analysis shows the branches distribution along the distance from the soma. (I) Total synapse number is compared on neurons over-expression MIR137 at DIV0 ($P = 0.0004$), DIV2 ($P = 0.053$) and DIV7 ($P = 0.092$). N indicates the number of independent observations (pups/nests) and n stands for number of neurons. In all boxplots, the lower and upper quartile represent observation outside of the 25–75 percentile range. The lower and upper whiskers represent the 10–90 percentile range. The boxes also show the median (–) and mean (+). * $P < 0.05$, ** $P < 0.01$, *** $P < 0.001$ are determined by multilevel test.

immunostaining). It remains to be determined how two studies, both in hippocampal neurons, produce such divergent experimental results and conclusions.

In summary, this study found multiple effects of miR-137 over-expression on synaptogenesis, pre-synaptic ultrastructure and -function, generally leading to reduced synapse density and function. Since dysfunctions in synaptic and neural circuit performance may be a central to many of the cardinal symptoms of schizophrenia (39,40), these effects may help to explain the association of genetic variation in *MIR137* and the concomitant increased expression reported for the disease-associated variant with schizophrenia (6). Reduced synapse number and function may impair network stability and performance and give rise to information processing abnormalities in schizophrenia (e.g. altered pre-pulse inhibition of acoustic startle, auditory evoked potential suppression and acoustic mismatch negativity) (41–43), and possibly the core symptoms of disorganized thinking and delusions. Because miR-137 is expressed from the stem cell stage onwards, the disease-associated SNP is also consistent with the idea that schizophrenia vulnerability emerges during development and is exposed by additional events, including environmental factors (the two-hit model). On the other hand, data from postmortem brain have suggested that the levels of important pre-synaptic proteins are higher rather than lower (as expected because the disease-associated SNP is reported to increase miR-137 expression) in postmortem brain of schizophrenia patients (44). Replication of the main findings, both of the levels of pre-synaptic proteins in postmortem tissue and functional effects of genetic variation in the *MIR-137* are required to reach consensus concepts to explain the association with schizophrenia.

In addition to schizophrenia, genetic variation in the *MIR-137* is also associated with several other traits/disorders, such as dorsolateral prefrontal cortex hyper-activation (45) and aberrant prefrontal-hippocampal functional connectivity (46). These disorders share several symptoms with schizophrenia. Pleiotropic effects on synapse formation and function and the possible consequences for network stability and performance induced by miR-137 dysregulation may be a common feature among multiple psychiatric disorders.

Materials and Methods

Laboratory animals

Primary hippocampal neurons were obtained from embryonic wildtype C57BL/6 mice at embryonic day 18 (E18), and cultured for 2 weeks. All animal procedures were performed according to protocols approved by the Vrije Universiteit Amsterdam.

Production of lenti-viral construct over-expressing *MIR-137* and *Syt-1*

The human *MIR137* sequence is 5'-GGCAGCGGCAGCTTGGTCC TCTGACTC-TCTTCGGTGACGGGTATTCTTGGGTGGATAATACGG ATTACGTTGTTATTGCTTAAGAATACGCGTAGTCGAGGAGAGTA CCAGCGGACGGGGGGCAGCGGCCGC-3'. Viral expression of *MIR-137* and scrambled was delivered using lenti-viral backbone pLL3.7 coupled to enhanced green fluorescent protein (EGFP) and expressed under a neuron-specific synapsin promoter. The synapsin core promoter contains no known miR-137 regulation sites. For *Syt1* overexpression, the *Syt1* cDNA was cloned into lenti-viral backbone with pIRES2-Cherry (Clontech) and expressed under the synapsin promoter. To construct these lenti-

viruses, HEK-293T cells were transfected with 8 µg lenti-virus plasmid, 4.8 µg VSV-G and 4.8 µg of each of the packaging plasmids pRSC-Rev and pMDL/pRRE using lipofectamine 2000 according to the manufacturer's protocol. Supernatant was collected 48 h later, centrifuged at 20 000 r.p.m. for 20 min, and the pellet resuspended in 50 µl Dulbecco's phosphate-buffered saline (Life Technologies) then aliquoted and stored at -80°C. The viral efficiency was measured by counting infected neurons showing EGFP fluorescence divided by the total of neurons.

Cell culture and virus infection

Hippocampal neurons were isolated from C57BL/6J wildtype E18 mice and prepared in two ways: glial island cultures and continental cultures. To overexpress *MIR137*, hippocampal neurons were infected by lenti-viral construct (described earlier) at three different time points: days *in vitro* 0 (DIV0, lamellipodium stage), DIV2 as the first neurites start to sprout, and the more mature developmental stage DIV7 (in this dynamic stage branches are expanding and regressing and there is apical branch specification). At DIV17, when fully developed, the neurons were fixed and stained as described below. Transfection efficiencies were 95–100%. To overexpress *Syt-1*, hippocampal neurons were infected with lenti-viral construct (described earlier) at DIV7, and used for patch clamp recording or immunostaining at DIV17.

Morphological analysis of neurons

Immunostaining of the neurons is performed using the primary antibodies MAP2 (chicken, 1:1000) for dendrite staining and vGlut1 (guinea pig, 1:4000) for synapse staining. For secondary antibodies, goat-anti-chicken (1:1000), goat-anti-guinea pig (1:1000) and goat-anti-mouse (1:1000) were used. For staining target proteins, Synaptotagmin 1 (1:2000, rabbit), Complexin 1 (1:2000, rabbit), Munc-18 (1:1000, rabbit), Rab3 (1:2000, rabbit) and PSD95 (1:800, rabbit) were used. Neuronal morphology was assessed by confocal microscopy and using the neurite and synapse detection program SynD (Schmitz et al. 2011). The neurons selected for imaging and analyzes showed a bright EGFP signal, indicating that they were infected with the shRNA lenti-viral construct. Only islands containing a single neuron forming excitatory synapses (autapses) were imaged and analyzed. The morphological characteristics measured were: average synapse number, total dendrite length, synapse density and synaptic protein levels of the proteins described earlier.

RNA isolation and cDNA synthesis

For RNA isolation, cells were homogenized in TRIzol (Invitrogen, Carlsbad, CA, USA) and total RNA was isolated using the QIAcube (QIAGEN, Venlo, The Netherlands) according to the manufacturers' specifications. RNA concentrations and purity were assessed by OD measurements at 260 and 280 nm on a NanoDrop spectrophotometer (Thermo Scientific). For cDNA synthesis, 1 µg of RNA and 125 pmol OligodT12 primer were dissolved in a total of 10 µl H₂O and incubated at 72°C for 10 min. Reverse transcriptase mix was added, consisting of 5 µl 5 × first-strand buffer (Invitrogen), 0.5 µl SuperScript II RNA polymerase (Invitrogen), 10 mM dNTPs, and 25 mM MgCl₂ in a total of 15 µl H₂O. The mixture was incubated at 42°C for 1 h, followed by 15 min at 70°C. cDNA quality was assessed on 0.8% agarose gel.

Electron microscopy

Hippocampal autaptic cultured neurons were fixed for 60 min at room temperature with 2.5% glutaraldehyde in 0.1 M cacodylate buffer (pH 7.4), post-fixed for 1 h at room temperature with 1% OsO₄/1% K₄Ru(CN)₆ in double distilled water. Following dehydration through a series of increasing ethanol concentrations, cells were embedded in Epon and polymerized for 24 h at 50°C. After polymerization of the Epon, the coverslip was removed by alternately dipping it in liquid nitrogen and hot water. Cells were selected by observing the Epon embedded autaptic culture under the light microscope, and mounted on pre-polymerized Epon blocks for thin sectioning. Ultrathin sections (~70 nm) were cut parallel to the cell monolayer and collected on single-slot, formvar-coated copper grids and stained in uranyl acetate and lead citrate.

Synapses were selected at low magnification using a JEOL 1010 electron microscope. All analyses were performed on single ultrathin sections of randomly selected synapses. The distribution of synaptic vesicles, total synaptic vesicle number and active zone length were measured by semi-automated custom written software running in Matlab (Mathworks, USA) on digital images of synapses taken at 100 000 × magnification using iTEM software (EMSIS, Germany). The observer was blinded to experimental condition. For all morphological analyses, we selected only synapses with intact synaptic plasma membranes with a recognizable pre- and post-synaptic density and clear synaptic vesicle membranes. Docked synaptic vesicles had no observation gap between the synaptic vesicle membrane to the active zone membrane (pixel size 0.52 nm). To get an estimate size of the total synaptic vesicle pool, distances of undocked synaptic membranes to the active zone membrane were also included in our measurement.

Synapse physiology

Whole-cell recordings were performed using an Axopatch 200B amplifier (Molecular Devices) at room temperature. Digidata 1440 and Clampex 10.0 (Molecular Devices) were used for data acquisition. The external solution contained (in mM): 140 NaCl, 2.4 KCl, 4 MgCl₂, 4 CaCl₂, 10 HEPES and 10 glucoses (pH 7.30, 300 mOsmol). Patch-pipette solution contained (in mM): 125 K⁺-gluconic acid, 10 NaCl, 4.6 MgCl₂, 15 creatine phosphate, 10 U/ml phosphocreatine kinase and 1 EGTA (pH 7.30). Only cells with an access resistance of <10 MΩ and leak current of <300 pA were accepted for analysis. The series-resistance for recording was compensated to 60%. To probe the asynchronous release during 40-Hz train stimulation for each stimulation a line was drawn from the initial and end point of the stimulus artifact to the initial point of the next one. The asynchronous part of response was defined as the current between this line and train baseline. The total charge of asynchronous release was obtained by integrating the asynchronous current from the 100 train stimuli at 40 Hz (47). The total charge is calculated by integrating the current corrected for baseline. All analyses were performed using Clampfit 10.2, MiniAnalysis (Synaptosoft) and custom software routines in Matlab R2010a. In action potential induced EPSC's the stimulation artifact was removed and interpolated using cubic interpolation.

Proteomics

Sample preparation: Hippocampal neuron cultures, infected at DIV0 with miR-137 over-expression lentivirus or scrambled

controls, were harvested for proteomic analysis at DIV17. The cells were washed two times with PBS, collected in tubes and centrifuged for 5 min at 3000g. The pellets were mixed with 5 × SDS sample buffer, heated to 98°C for 5 min, and 3 μl 30% acrylamide was added to alkylate cysteine residues. Proteins were separated on a 10% SDS polyacrylamide gel and stained with Coomassie Blue. Each sample lane was cut, de-stained and the proteins digested with trypsin overnight at 37°C. Finally, the peptides were dried, re-dissolved in 7 μl 2% acetonitrile, 0.1% formic acid for the subsequence LC-MS/MS analysis (48).

Micro-LC and SWATH mass spectrometry: Peptides were analyzed by micro LC MS/MS using an Ultimate 3000 LC system (Dionex, Thermo Scientific) coupled to the TripleTOF 5600 mass spectrometer (Sciex). Peptides were trapped on a 5 mm Pepmap 100 C18 column (300 μm i.d., 5 μm particle size, Dionex), and fractionated on a 200 mm Alltima C18 column (100 μm i.d., 3 μm particle size). The acetonitrile concentration in the mobile phase was increased from 5 to 18% in 88 min, to 25% at 98 min, 40% at 108 min and to 90% in 2 min, at a flow rate of 5 μl/min. The eluted peptides were electro-sprayed into the TripleTOF MS, with a micro-spray needle voltage of 5500 V. SWATH experiments consisted of a parent ion scan of 150 ms followed by SWATH window of 8 Da with scan time of 80 ms, and stepped through the mass range between 450 and 770 m/z. The collision energy for each window was determined based on the appropriate collision energy for a 2+ ion, centered upon the window with a spread of 15 eV.

SWATH data analysis: The data were analyzed using Spectronaut 8.0 (49). The spectral library was created from merging of two data-dependent analyses of non-transfected hippocampal neuron culture and hippocampal synaptosomes containing spike-in iRT peptides from Biognosys. The retention time prediction was set to dynamic iRT; the cross-run normalization based on total peak areas was enabled. Peptide abundances were exported and processed using R language for statistical computation. Only peptides present in both transfected and control groups and quantified with high confidence were used (i.e. a Q-value ≤ 10⁻⁴ over all samples in either group, allowing for one outlier within each condition). Protein abundances were computed using Spectronaut normalized peak area, and Loess normalized using the 'normalizeCyclicLoess' function from limma R package (fast method and 10 iterations) (50).

Empirical Bayes moderated t-statistics with multiple testing correction by FDR was performed on log-transformed protein abundances as implemented by the 'eBayes' and 'topTable' functions from limma R package. An FDR adjusted threshold of 0.05 was used to discriminate significantly regulated proteins.

eQTL analysis

The results from the most recent large schizophrenia GWAS (2) were compared with results from the GTEx project (Lonsdale et al., 2013; v6). GTEx expression results are reported for a selection of genetic variants based on three criteria. First, only variants within the MIR137 GWAS locus (98.30–98.55 Mb on chromosome 1, hg19) were considered. Second, variants were required to be available in the schizophrenia GWAS results, the GTEx project, as well as the 1000 Genomes Project phase 3 reference panel (51). The 1000 Genomes data were used as a reference panel to compute the correlation (r^2) between genetic variants in subjects of European descent. Third, only genetic variants in high linkage disequilibrium ($r^2 > 0.6$) with the GWAS

top variant of the *MIR137* locus (rs1702295) were selected for expression analysis. Subsequently, effect alleles were aligned between the GWAS and GTEx results, defining the risk increasing allele in the schizophrenia GWAS as effect alleles in the GTEx results. Within the region of interest, only expression results for the *MIR137* host gene (*MIR137HG*) were available in GTEx. Association between the selected schizophrenia risk alleles with expression of *MIR137HG* in 10 tissues (Testis, pituitary, ovary, cell transformed fibroblasts, basal ganglia, hypothalamus, hippocampus, cortex, caudate basal ganglia and adrenal), eight of which were brain regions extracted from the GTEx results.

Statistics

Data are presented as mean values \pm S.E.M., with N referring to the number of independent observations (mice/nests), n referring to the total number of observations (cells) from each group. Statistical analysis was performed with SPSS (Version 20.0, Armonk, NY). To test two groups, an unpaired t-test (with Welch correction if SDs are not equal) was used to determine statistical significance. To test multiple groups, we used one-way analysis of variance (ANOVA). For the analysis of electron microscopy and immunostaining data, a multilevel comparison was used to accommodate nested data (synapses originating from the same neuron) (Aarts et al., 2014).

Acknowledgements

The authors thank Sara Grasman for immunocytochemical experiments and morphometry and Rien Dekker for the electron microscopy. We also thank Dr Ronald E. van Kesteren and Dr Pim van Nierop for discussion of the project. We thank Rob Zwart and Marieke van Ziel for their help on qPCR experiment.

Conflict of Interest statement. None declared.

Funding

This work was supported by the Swedish Research Council (VR Dnr: 538–2013-8865 to P.F.S.), the European Union (ERC Advanced grant 322966 to M.V.; HEALTH-F2–2009-241498 EUROSPIN to M.V. and HEALTH-F2–2009-242167 SynSys to A.B.S. and M.V.), The Netherlands Organization for Scientific Research (NWO VICI 453–14-005 to D.P.). The Genotype-Tissue Expression (GTEx) Project was supported by the Common Fund of the Office of the Director of the National Institutes of Health, and by NCI, NHGRI, NHLBI, NIDA, NIMH and NINDS. The data used for the analyses described in this article were obtained from the GTEx Portal on February 17, 2016. Funding to pay the Open Access publication charges for this article was provided by Section of Functional Genomics, Faculty of Science, Vrije Universiteit Amsterdam.

References

- Polderman, T.J.C., Benyamin, B., de Leeuw, C.A., Sullivan, P.F., van Bochoven, A. and Visscher, P.M. (2015) Meta-analysis of the heritability of human traits based on fifty years of twin studies. *Nat. Genet.*, **47**, 702–709.
- Ripke, S., Neale, B.M., Corvin, A., Walters, J.T., Farh, K.-H., Holmans, P.A., Lee, P., Bulik-Sullivan, B., Collier, D.A., Huang, H. et al. (2014) Biological insights from 108 schizophrenia-associated genetic loci. *Nature*, **511**, 421–427.
- Consortium TSPG-WAS (GWAS). (2011) Genome-wide association study identifies five new schizophrenia loci. *Nat. Genet.*, **43**, 969–976.
- Willemsen, M.H., Vallès, A., Kirkels, L.A.M.H., Mastebroek, M., Loohuis, N.O., Kos, A., Wissink-Lindhout, W.M., de Brouwer, A.P., Nillesen, W.M., Pfundt, R. et al. (2011) Chromosome 1p21.3 microdeletions comprising *DPYD* and *MIR137* are associated with intellectual disability. *J. Med. Genet.*, **48**, 810–818.
- Bartel, D.P. (2009) MicroRNAs: target recognition and regulatory functions. *Cell*, **136**, 215–233.
- Siegert, S., Seo, J., Kwon, E.J., Rudenko, A., Cho, S., Wang, W., Flood, Z., Martorell, A.J., Ericsson, M., Mungenast, A.E. et al. (2015) The schizophrenia risk gene product miR-137 alters presynaptic plasticity. *Nat. Neurosci.*, **18**, 1008–1016.
- Sun, GQiang, Ye, P., Murai, K., Lang, M.-F., Li, S., Zhang, H., Li, W., Fu, C., Yin, J., Wang, A. et al. (2011) miR-137 forms a regulatory loop with nuclear receptor TLX and LSD1 in neural stem cells. *Nat. Commun.*, **2**, 529.
- Sakamoto, K. and Crowley, J.J. (2017) A comprehensive review of the genetic and biological evidence supports a role for MicroRNA-137 in the etiology of schizophrenia. *Am. J. Med. Genet. B Neuropsychiatr. Genet.*, **9999**, 1–15.
- Silber, J., Lim, D.A., Petritsch, C., Persson, A.I., Maunakea, A.K., Yu, M., Vandenberg, S.R., Ginzinger, D.G., James, C.D., Costello, J.F. et al. (2008) miR-124 and miR-137 inhibit proliferation of glioblastoma multiforme cells and induce differentiation of brain tumor stem cells. *BMC Med.*, **6**, 14.
- Smrt, R.D., Szulwach, K.E., Pfeiffer, R.L., Li, X., Guo, W., Pathania, M., Teng, Z.-Q., Luo, Y., Peng, J., Bordey, A. et al. (2010) MicroRNA miR-137 regulates neuronal maturation by targeting ubiquitin ligase mind bomb-1. *Stem Cells*, **28**, 1060–1070.
- Crowley, J.J., Collins, A.L., Lee, R.J., Nonneman, R.J., Farrell, M.S., Ancalade, N., Mugford, J.W., Agster, K.L., Nikolova, V.D., Moy, S.S. and Sullivan, P.F. (2015) Disruption of the miR-137 primary transcript results in early embryonic lethality in mouse. *Biol. Psychiatry*, **77**, e5–e7.
- Spronsen, M. van, Battum, E.Y. van, Kuijpers, M., Vangoor, V.R., Rietman, M.L., Pothof, J., Gumy, L.F., van Ijcken, W.F., Akhmanova, A., Pasterkamp, R.J., Hoogenraad, C.C. (2013) Developmental and activity-dependent miRNA expression profiling in primary hippocampal neuron cultures. *Plos One*, **8**, e74907.
- Boudreau, R.L., Jiang, P., Gilmore, B.L., Spengler, R.M., Tirabassi, R., Nelson, J.A., Ross, C.A., Xing, Y. and Davidson, B.L. (2014) Transcriptome-wide discovery of microRNA binding sites in human brain. *Neuron*, **81**, 294–305.
- Collins, A.L., Kim, Y., Bloom, R.J., Kelada, S.N., Sethupathy, P. and Sullivan, P.F. (2014) Transcriptional targets of the schizophrenia risk gene *MIR137*. *Transl. Psychiatry*, **4**, 404.
- Hill, M.J., Donocik, J.G., Nuamah, R.A., Mein, C.A., Sainz-Fuertes, R. and Bray, N.J. (2014) Transcriptional consequences of schizophrenia candidate miR-137 manipulation in human neural progenitor cells. *Schizophr. Res.*, **153**, 225–230.
- Olde Loohuis, N.F.M., Nadif Kasri, N., Glennon, J.C., van Bokhoven, H., Hébert, S.S., Kaplan, B.B. et al. The schizophrenia risk gene *MIR137* acts as a hippocampal gene network node orchestrating the expression of genes relevant to nervous system development and function. *Prog. Neuropsychopharmacol. Biol. Psychiatry*, **73**, 109–118.
- Strazisar, M., Cammaerts, S., van der Ven, K., Forero, D.A., Lenaerts, A.-S., Nordin, A., Almeida-Souza, L., Genovese, G., Timmerman, V., Liekens, A. et al. (2015) *MIR137* variants identified in psychiatric patients affect synaptogenesis and neuronal transmission gene sets. *Mol. Psychiatry*, **20**, 472–481.

18. Tamim, S., Vo, D.T., Uren, P.J., Qiao, M., Bindewald, E., Kasprzak, W.K., Shapiro, B.A., Nakaya, H.I., Burns, S.C., Araujo, P.R. et al. (2014) Genomic analyses reveal broad impact of miR-137 on genes associated with malignant transformation and neuronal differentiation in glioblastoma cells. *PLOS One*, **9**, 85591.
19. Wright, C., Turner, J.A., Calhoun, V.D. and Perrone-Bizzozero, N. (2013) Potential impact of miR-137 and its targets in schizophrenia. *Front. Behav. Psychiatr. Genet.*, **4**, 58.
20. Kwon, E., Wang, W. and Tsai, L.-H. (2013) Validation of schizophrenia-associated genes CSMD1, C10orf26, CACNA1C and TCF4 as miR-137 targets. *Mol. Psychiatry*, **18**, 11–12.
21. Ebert, M.S., Neilson, J.R. and Sharp, P.A. (2007) MicroRNA sponges: competitive inhibitors of small RNAs in mammalian cells. *Nat. Methods*, **4**, 721–726.
22. Olde Loohuis, N.F.M., Ba, W., Stoerchel, P.H., Kos, A., Jager, A., Schratz, G., Martens, G.J.M., van Bokhoven, H., Nadif Kasri, N., Aschrafi, A. et al. (2015) MicroRNA-137 controls AMPA-receptor-mediated transmission and mGluR-dependent LTD. *Cell Rep.*, **11**, 1876–1884.
23. Verma, P., Augustine, G.J., Ammar, M.-R., Tashiro, A. and Cohen, S.M. (2015) A neuroprotective role for microRNA miR-1000 mediated by limiting glutamate excitotoxicity. *Nat. Neurosci.*, **18**, 379–385.
24. Szulwach, K.E., Li, X., Smrt, R.D., Li, Y., Luo, Y., Lin, L., Santistevan, N.J., Li, W., Zhao, X., Jin, P. et al. (2010) Cross talk between microRNA and epigenetic regulation in adult neurogenesis. *J. Cell. Biol.*, **189**, 127–141.
25. Saba, R., Störchel, P.H., Aksoy-Aksel, A., Kepura, F., Lippi, G., Plant, T.D. and Schratz, G.M. (2012) Dopamine-regulated MicroRNA MiR-181a controls GluA2 surface expression in hippocampal neurons. *Mol. Cell Biol.*, **32**, 619–632.
26. Schratz, G.M., Tuebing, F., Nigh, E.A., Kane, C.G., Sabatini, M.E., Kiebler, M. and Greenberg, M.E. (2006) A brain-specific microRNA regulates dendritic spine development. *Nature*, **439**, 283–289.
27. Cohen, J.E., Lee, P.R., Chen, S., Li, W. and Fields, R.D. (2011) MicroRNA regulation of homeostatic synaptic plasticity. *Proc. Natl. Acad. Sci. U.S.A.*, **108**, 1650–11655.
28. Südhof, T.C. (2013) Neurotransmitter release: the last millisecond in the life of a synaptic vesicle. *Neuron*, **80**, 675–690.
29. Fromer, M., Roussos, P., Sieberts, S.K., Johnson, J.S., Kavanagh, D.H. et al. (2016) Gene expression elucidates functional impact of polygenic risk for schizophrenia. *Nat Neuroscience*, **19**, 1442–1453.
30. GTEx Consortium. (2015) The Genotype-Tissue Expression (GTEx) pilot analysis: multitissue gene regulation in humans. *Science*, **348**, 648–660.
31. Imig, C., Min, S.-W., Krinner, S., Arancillo, M., Rosenmund, C., Südhof, T.C., Rhee, J., Brose, N. and Cooper, B.H. (2014) The morphological and molecular nature of synaptic vesicle priming at presynaptic active zones. *Neuron*, **84**, 416–431.
32. de Wit, H., Walter, A.M., Milosevic, I., Gulyás-Kovács, A., Riedel, D., Sørensen, J.B. and Verhage, M. (2009) Synaptotagmin-1 docks secretory vesicles to syntaxin-1/SNAP-25 acceptor complexes. *Cell*, **38**, 935–946.
33. Toonen, R.F.G., Wierda, K., Sons, M.S., Wit, H. de, Cornelisse, L.N., Brussaard, A., Plomp, J.J. and Verhage, M. (2006) Munc18-1 expression levels control synapse recovery by regulating readily releasable pool size. *Proc. Natl. Acad. Sci. U.S.A.*, **103**, 18332–18337.
34. Crabtree, G.W. and Gogos, J.A. (2014 Nov) Synaptic plasticity, neural circuits, and the emerging role of altered short-term information processing in schizophrenia. *Front. Synaptic Neurosci.*, **6**, 1–27.
35. Egbujo, C.N., Sinclair, D. and Hahn, C.-G. (2016) Dysregulations of synaptic vesicle trafficking in schizophrenia. *Curr. Psychiatry Rep.*, **18**, 77.
36. Brockhaus-Dumke, A., Schultze-Lutter, F., Mueller, R., Tendolkar, I., Bechdolf, A., Pukrop, R., Klosterkoetter, J. and Ruhrmann, S. (2008) Sensory gating in schizophrenia: p 50 and N100 gating in antipsychotic-free subjects at risk, first-episode, and chronic patients. *Biol. Psychiatry*, **64**, 376–384.
37. Clementz, B.A., Geyer, M.A. and Braff, D.L. (1998) Poor P50 suppression among schizophrenia patients and their first-degree biological relatives. *Am. J. Psychiatry*, **155**, 1691–1694.
38. Swerdlow, N.R., Light, G.A., Cadenhead, K.S., Sprock, J., Hsieh, M.H. and Braff, D.L. (2006) Startle gating deficits in a large cohort of patients with schizophrenia: relationship to medications, symptoms, neurocognition, and level of function. *Arch. Gen. Psychiatry*, **63**, 1325–1335.
39. Ramos-Miguel, A., Beasley, C.L., Dwork, A.J., Mann, J.J., Rosoklija, G., Barr, A.M. and Honer, W.G. (2015) Increased SNARE protein-protein interactions in orbitofrontal and anterior cingulate cortices in schizophrenia. *Biol. Psychiatry*, **78**, 361–373.
40. van Erp, T.G.M., Guella, I., Vawter, M.P., Turner, J., Brown, G.G., McCarthy, G., Greeve, D.N., Glover, G.H., Calhoun, V.D., Lim, K.O. et al. (2014) Schizophrenia miR-137 locus risk genotype is associated with dorsolateral prefrontal cortex hyperactivation. *Biol. Psychiatry*, **75**, 398–405.
41. Liu, B., Zhang, X., Hou, B., Li, J., Qiu, C., Qin, W., Yu, C. and Jiang, T. (2014) The impact of MIR137 on dorsolateral prefrontal-hippocampal functional connectivity in healthy subjects. *Neuropsychopharmacology*, **39**, 2153–2160.
42. Hagler, D.J. and Goda, Y. (2001) Properties of synchronous and asynchronous release during pulse train depression in cultured hippocampal neurons. *J. Neurophysiol.*, **85**, 2324–2334.
43. Wan, L., Chen, N., Klemmer, P., Koopmans, F., Karupothula, R. and Smit, A.B. (2012) Identifying true protein complex constituents in interaction proteomics: the example of the DMXL2 protein complex. *Proteomics*, **12**, 2428–2432.
44. Bruderer, R., Bernhardt, O.M., Gandhi, T., Miladinović, S.M., Cheng, L.-Y., Messner, S., Ehrenberger, T., Zanotelli, V., Butscheid, Y., Escher, C. et al. (2015) Extending the limits of quantitative proteome profiling with data-independent acquisition and application to acetaminophen-treated three-dimensional liver microtissues. *Mol. Cell Proteomics*, **14**, 1400–1410.
45. Ritchie, M.E., Phipson, B., Wu, D., Hu, Y., Law, C.W., Shi, W. and Smyth, G.K. (2015) Limma powers differential expression analyses for RNA-sequencing and microarray studies. *Nucleic Acids Res.*, **43**, 47.
46. The 1000 Genomes Project Consortium. (2015) A global reference for human genetic variation. *Nature*, **526**, 68–74.
47. Furshpan, E.J., MacLeish, P.R., O'Lague, P.H. and Potter, D.D. (1976) Chemical transmission between rat sympathetic neurons and cardiac myocytes developing in microcultures:

- evidence for cholinergic, adrenergic, and dual-function neurons. *Proc. Natl. Acad. Sci. U.S.A.*, **73**, 4225–4229.
48. Wierda, K.D.B., Toonen, R.F.G., de Wit, H., Brussaard, A.B. and Verhage, M. (2007) Interdependence of PKC-dependent and PKC-independent pathways for presynaptic plasticity. *Neuron*, **54**, 75–290.
49. Doerr, A. (2015) DIA mass spectrometry. *Nat. Methods*, **12**, 35–35.
50. Rouillard, A.D., Gundersen, G.W., Fernandez, N.F., Wang, Z., Monteiro, C.D. and McDermott, M.G. (2016) The harmonizome: a collection of processed datasets gathered to serve and mine knowledge about genes and proteins. *Database*, **3**, 1–16.
51. Harraz, M.M., Eacker, S.M., Wang, X., Dawson, T.M. and Dawson, V.L. (2012) MicroRNA-223 is neuroprotective by targeting glutamate receptors. *Proc. Natl. Acad. Sci. U.S.A.*, **109**, 18962–18967.